ACTIVE CONTOUR and SEGMENTATION MODELS USING GEOMETRIC PDE's for MEDICAL IMAGING ⋆

Tony F. Chan and Luminita A. Vese

Department of Mathematics, University of California, Los Angeles,
405 Hilgard Avenue, Los Angeles, CA 90095-1555, U.S.A.
E-mail: chan@ipam.ucla.edu, lvese@math.ucla.edu

Abstract. This paper is devoted to the analysis and the extraction of information from bio-medical images. The proposed technique is based on object and contour detection, curve evolution and segmentation. We present a particular active contour model for 2D and 3D images, formulated using the level set method, and based on a 2-phase piecewise-constant segmentation. We then show how this model can be generalized to segmentation of images with more than two segments. The techniques used are based on the Mumford-Shah [21] model. By the proposed models, we can extract in addition measurements of the detected objects, such as average intensity, perimeter, area, or volume. Such informations are useful when in particular a time evolution of the subject is known, or when we need to make comparisons between different subjects, for instance between a normal subject and an abnormal one. Finally, all these will give more informations about the dynamic of a disease, or about how the human body growths. We illustrate the efficiency of the proposed models by calculations on two-dimensional and three-dimensional bio-medical images.

1 Introduction

Techniques of image processing and data analysis are more and more used in the medical field. Mathematical algorithms of feature extraction, modelization and measurements can exploit the data to detect pathology in an individual or patient group, the evolution of the disease, or to compare a normal subject to an abnormal one.

In this paper, we show how the active contour model without edges introduced in [7], and its extension to segmentation of images from [8], can be applied to medical images. The benefits of these algorithms can be summarized in: automatically detecting interior contours, robust with respect to noise, ability to detect and represent complex topologies (boundaries, segments), and finally, extraction of geometric measurements, such as length, area, volume, intensity, of a detected contour, surface or region, respectively. These informations can be later used to study the evolution in time of a

⋆ This work was supported in part by ONR Contract N00014-96-1-0277 and NSF Contract DMS-9973341.

disease (a growing tumor), or to compare two different subjects, usually a normal one and an abnormal one.

In active contours, the basic idea is to evolve a curve C in a given image u_0, and to stop the evolution when the curve meets an object or a boundary of the image. In order to stop the curve on the desired objects, classical models use the magnitude of the gradient of the image, to detect the boundaries of the object. Therefore, these models can detect only edges defined by gradient. Some of these classical models suffer from other limitations: the initial curve has to surround the objects to be detected, and interior contours cannot be detected automatically. We refer the reader to [9], [3], [16], [17] [18], [4], [10], for a few examples of active contour models based on the gradient for the stopping criteria.

The active contour model that we will use here [7], is different than the classical ones, because it is not based on the gradient (a local information) for the stopping criteria. Instead, it is based on a global segmentation of the image, and it has the advantages mentioned above. For the implementation of the active contour model , the level set method of S. Osher and J. Sethian [22] has been efficiently used. We have also extended this model to segment images, based on the piecewise-constant Mumford-Shah model [21], using a particular multiphase level set formulation [8]. This formulation allows for multiple segments, triple junctions, complex topologies and in addition, compared with other multiphase level set formulations, the problems of vacuum and overlap of phases cannot arise.

Before going further, we would like to refer the reader to other works on segmentation using Mumford-Shah techniques: [1], [2], [5], [6], [12], [19], [20], [23], [25], [26], [28], [30], [31], and to related works with applications to medical imagery: [27], [14], [15], [11], [24], [13].

We will first recall the active contour model without edges from [7], and its extension to segmentation of images [8]. Then, we will illustrate how these geometric PDE models can be applied to segmentation of medical images.

2 Description of the models

Let us first introduce our notations. Let $\Omega \subset I\!\!R^n \to I\!\!R$ be an open and bounded set, and let $u_0 : \overline{\Omega} \to I\!\!R$ be a given image. In our case, we will consider $n = 2$ (plane images), and $n = 3$ (volumetric images), and $x \in I\!\!R^n$ denotes an arbitrary point. Let $C \subset \Omega$ be a hyper-surface, as the boundary of an open subset ω of Ω, i.e. ω is open, $\omega \subset \Omega$ and $C = \partial\omega$. We call "$inside(C)$" the region given by ω, and "$outside(C)$" the region given by $\Omega \setminus \overline{\omega}$. We recall that $\mathcal{H}^{n-1}$ denotes the $(n-1)$-dimensional Hausdorff measure in $I\!\!R^n$. For $n = 2$, $\mathcal{H}^{n-1}(C)$ gives the length of the curve C, and for $n = 3$, $\mathcal{H}^{n-1}(C)$ gives the area of the surface C.

In this paper, we consider the problem of active contours and object detection, via the level set method [22] and Mumford-Shah segmentation

[21]. Giving an initial hyper-surface C, we evolve it under some constraints, in order to detect objects in the image u_0. In addition, we also obtain a segmentation of the image, given by the connected components of $\Omega \setminus C$ and the averages of u_0 in these regions. Finally, we would like to extract more informations, in the form of geometrical measurements for the detected objects.

We introduce an energy based segmentation, as a particular case of the minimal partition problem of Mumford-Shah [21]. As in [7], we denote by c_1 and c_2 two unknown constants, representing the averages of the image u_0 inside C and outside C, respectively. A variant of the model introduced in [7], but generalized to n dimensions, is:

$$\inf_{c_1,c_2,C} F(c_1,c_2,C), \tag{1}$$

where, using the above notations,

$$F(c_1,c_2,C) = \lambda_1 \int_{inside(C)} (u_0(x)-c_1)^2 dx + \lambda_2 \int_{outside(C)} (u_0(x)-c_2)^2 dx \\ + \mu \mathcal{H}^{n-1}(C) + \nu \mathcal{L}^n(inside(C)).$$

Here, $\mathcal{L}^n$ denotes the Lebesgue measure in $\mathbb{R}^n$. For $n=2$, $\mathcal{L}^2(\omega)$ denotes the area of ω, and for $n=3$, $\mathcal{L}^3(\omega)$ denotes the volume of ω. The coefficients $\lambda_1, \lambda_2, \mu$ and ν are fixed non-negative constants.

Minimizing the above energy with respect to c_1, c_2 and C, leads to an active contour model, based on segmentation. It looks for the best simplest approximation of the image taking only two values, c_1 and c_2, and the active contour is the boundary between the two corresponding regions. One of the regions represents the objects to be detected, and the other region gives the background. We note that, when $\lambda_1 = \lambda_2 = 1$ and $\nu = 0$, the minimization of the above energy is a particular case of the piecewise-constant Mumford-Shah model for segmentation [21].

For the evolving curve C, we use an implicit representation given by the level set method of S. Osher and J. Sethian [22], because it has many advantages, comparing with an explicit parameterization: it allows for automatic change of topology, cusps, merging and breaking, and the calculations are made on a fix rectangular grid. In this framework, as in [22], a hyper-surface $C \in \Omega$ is represented implicitly via a Lipschitz function $\phi : \Omega \to \mathbb{R}$, such that: $C = \{x \in \Omega | \phi(x) = 0\}$. Also, ϕ needs to have opposite signs on each side of C. For instance, we can choose $\phi(x) > 0$ inside C (i.e. in ω), and $\phi(x) < 0$ outside C (i.e. in $\Omega \setminus \overline{\omega}$).

As in [7], also following [29], we can formulate the above active contour model in terms of level sets. We therefore replace the unknown variable C by the unknown variable ϕ. Using the Heaviside function H defined by:

$$H(z) = \begin{cases} 1, & \text{if } z \geq 0 \\ 0, & \text{if } z < 0, \end{cases}$$

we express the terms in the energy F in the following way:

$$F(c_1,c_2,\phi) = \lambda_1 \int_{\phi>0} (u_0(x)-c_1)^2 dx + \lambda_2 \int_{\phi<0} (u_0(x)-c_2)^2 dx$$
$$+ \mu\mathcal{H}^{n-1}(C) + \nu\mathcal{L}^n(C),$$

or

$$F(c_1,c_2,\phi) = \lambda_1 \int_{\Omega} (u_0(x)-c_1)^2 H(\phi(x))dx$$
$$+\lambda_2 \int_{\Omega} (u_0(x)-c_2)^2 (1-H(\phi(x))dx + \mu \int_{\Omega} |\nabla H(\phi(x))| + \nu \int_{\Omega} H(\phi(x))dx.$$

Considering H_ε and δ_ε any C^1 approximations and regularizations of the Heaviside function H and Delta function δ_0, as $\varepsilon \to 0$, and with $H'_\varepsilon = \delta_\varepsilon$, and minimizing the energy with respect to c_1, c_2, and ϕ, we obtain:

$$c_1 = \frac{\int_\Omega u_0(x)H(\phi(x))dx}{\int_\Omega H(\phi(x))dx}, \; c_2 = \frac{\int_\Omega u_0(x)(1-H(\phi(x)))dx}{\int_\Omega (1-H(\phi(x)))dx},$$

and

$$\frac{\partial \phi}{\partial t} = \delta_\varepsilon(\phi)\Big[\mathrm{div}\Big(\frac{\nabla\phi}{|\nabla\phi|}\Big) - \lambda_1(u_0-c_1)^2 + \lambda_2(u_0-c_2)^2 - \nu\Big].$$

We see that c_1 and c_2 are the averages of the image u_0 inside C and outside C respectively. Solving the equation in ϕ by an iterative scheme, we implicitly move the curve C toward boundaries in the image. The motion of the curve is governed by the mean curvature $\mathrm{div}\Big(\frac{\nabla\phi}{|\nabla\phi|}\Big)$ and by terms depending on u_0. In the end, we also obtain a two-phase segmentation of the image, given by $u(x) = c_1 H(\phi(x)) + c_2(1-H(\phi(x)))$.

This model can be extended to the general piecewise-constant Mumford-Shah segmentation model [21] (when we look for more than two segments), originally proposed in two dimensions. It minimizes the energy

$$F^{MS}(u,C) = \sum_i \int_{\Omega_i} (u_0(x)-c_i)^2 dx + \mu\mathcal{H}^{n-1}(C), \tag{2}$$

where $u = c_i$ inside each connected component of $\Omega \setminus C$.

In order to find a piecewise-constant approximation of u_0 based on the above Mumford-Shah model and level sets, we propose a multiphase level set representation, which allows for multiple segments and triple junctions. The basic idea is to use several level set functions. In [29] for instance, one level set function is associated to each phase. But in our formulation, we considerably reduce the number of level set functions, in the following way. As we have seen, using one level set function ϕ, we can partition the domain Ω in up to two disjoint regions, given by $\{\phi > 0\}$ and $\{\phi < 0\}$. Using two level set functions ϕ_1, ϕ_2, we can partition the domain in up to four disjoint regions, given by $\{\phi_1 > 0, \phi_2 > 0\}$, $\{\phi_1 > 0, \phi_2 < 0\}$, $\{\phi_1 < 0, \phi_2 > 0\}$, and $\{\phi_1 < 0, \phi_2 < 0\}$; and so on, using n level set functions $\phi_1, ..., \phi_n$, we can define up to 2^n regions or phases. These are disjoint (no overlap) and form a covering of Ω (no vacuum).

Let us write the associated energy for $n = 2$ level set functions, for instance, for the purpose of illustration (see [8] for more general cases):

$$\begin{aligned} F(c, \Phi) = &\int_\Omega (u_0(x) - c_{11})^2 H(\phi_1(x)) H(\phi_2(x)) dx \\ &+ \int_\Omega (u_0(x) - c_{10})^2 H(\phi_1(x))(1 - H(\phi_2(x))) dx \\ &+ \int_\Omega (u_0(x) - c_{01})^2 (1 - H(\phi_1(x))) H(\phi_2(x)) dx \\ &+ \int_\Omega (u_0(x) - c_{00})^2 (1 - H(\phi_1(x)))(1 - H(\phi_2(x))) dx \\ &+ \mu \int_\Omega |\nabla H(\phi_1(x))| + \mu \int_\Omega |\nabla H(\phi_2(x))|, \end{aligned}$$

where $c = (c_{11}, c_{10}, c_{01}, c_{00})$, $\Phi = (\phi_1, \phi_2)$.

With these notations, we can express the image-function u as:

$$\begin{aligned} u(x) = &\, c_{11} H(\phi_1(x)) H(\phi_2(x)) + c_{10} H(\phi_1(x))(1 - H(\phi_2(x))) \\ &+ c_{01}(1 - H(\phi_1(x))) H(\phi_2(x)) + c_{00}(1 - H(\phi_1(x)))(1 - H(\phi_2(x))). \end{aligned}$$

The Euler-Lagrange equations obtained by minimizing $F(c, \Phi)$ with respect to c and Φ are:

$$\begin{cases} c_{11} = mean(u_0) \text{ in } \{\phi_1 > 0, \phi_2 > 0\} \\ c_{10} = mean(u_0) \text{ in } \{\phi_1 > 0, \phi_2 < 0\} \\ c_{01} = mean(u_0) \text{ in } \{\phi_1 < 0, \phi_2 > 0\} \\ c_{00} = mean(u_0) \text{ in } \{\phi_1 < 0, \phi_2 < 0\}, \end{cases} \tag{3}$$

$$\frac{\partial \phi_1}{\partial t} = \delta_\varepsilon(\phi_1) \Big\{ \mu \text{div}\Big(\frac{\nabla \phi_1}{|\nabla \phi_1|}\Big) - \Big[\Big((u_0 - c_{11})^2 - (u_0 - c_{01})^2\Big) H(\phi_2) \tag{4}$$

$$+ \Big((u_0 - c_{10})^2 - (u_0 - c_{00})^2\Big)(1 - H(\phi_2))\Big]\Big\}, \tag{5}$$

and

$$\frac{\partial \phi_2}{\partial t} = \delta_\varepsilon(\phi_2) \Big\{ \mu \text{div}\Big(\frac{\nabla \phi_2}{|\nabla \phi_2|}\Big) - \Big[\Big((u_0 - c_{11})^2 - (u_0 - c_{01})^2\Big) H(\phi_1) \tag{6}$$

$$+ \Big((u_0 - c_{10})^2 - (u_0 - c_{00})^2\Big)(1 - H(\phi_1))\Big]\Big\}. \tag{7}$$

We note that the equations in $\Phi = (\phi_1, \phi_2)$ are governed by both mean curvature and jump of the data energy terms across the boundary.

After each calculation, we can extract the length or the area of the evolving contour or surface using the formula $\int_\Omega |\nabla H(\phi(x))|dx$, the area or the volume of the detected objects (integrating the characteristic functions of each component of the partition), and the average intensity of the image u_0 inside the object, given by the computed constants.

3 Applications to bio-medical images

In this section, we show how the previous active contour model without edges and its extension to segmentation can be applied to medical images. In our numerical results, $\lambda_1 = \lambda_2 = 1$ and $\nu = 0$. The only varying parameter is μ, the coefficient of the length term, which has a scaling role. We will use the notations A_i (or V_i) for the area (or the volume) of the region given by c_i, by L (or L_i) for the perimeter of the same region, and by A the area of the active surface in 3D, and so on. In most of the experimental results we have $\lambda_1 = \lambda_2 = 1$ and $\nu = 0$, except for those from Figure 2, where $\nu > 0$ and $\lambda_1 > \lambda_2$.

In Figure 1, we consider an image representing bone tissues. We perform the active contour model, and we show the evolving curve, together with the segmented image u, given by c_1 if $\phi > 0$ and c_2 if $\phi < 0$. We illustrate here that interior contours are automatically detected, also that complex shapes can be detected, with blurred boundaries. Here, $\mu = 0.001 \cdot 255^2$, $c_1 = 218$, $c_2 = 115$, $A_1 = 22368$, $A_2 = 17830$, $L = 2171.49$.

In Figure 2, we show how a tumor with blurred boundaries can be detected, in an MRI brain data, using the active contour model without edges.

In Figure 3 we show an active surface ($n = 3$), to detect the boundary in a brain MRI volumetric image. We only show a part of the surface, in a 61x61x61 cube. Again, we can extract the area of the detected surface boundary, and the enclosed volume. In Figure 3 we show cross-sections of the 3D results: the evolving curve in a slice. We also show the final segmentation. Here, $\mu = 0.01 \cdot 255^2$. The final geometric quantities are: $c_1 = 164$, $c_2 = 1$, $V_1 = 304992$, $V_2 = 1194140$, $A = 69682.5$.

Finally, in Figures 5 and 6 we apply the four-phase segmentation model, using two level set functions, again on a MRI brain image. Here, four phases are detected (see Figure 4), and in Figure 5 we show the evolution of the curves, together with the corresponding piecewise-constant segmentations ($\mu = 0.01 \cdot 255^2$, $c_{11} = 45$, $c_{10} = 159$, $c_{01} = 9$, $c_{00} = 103$, $A_{11} = 2572$, $A_{10} = 6656$, $A_{01} = 11401$, $A_{00} = 8874$, $L_{11} = 2063$, $L_{10} = 3017$, $L_{01} = 3749$, $L_{00} = 5250$).

4 Concluding remarks

In this paper, we have shown how the geometric PDE models from [7] and [8] can be applied to segmentation and feature extraction for medical images.

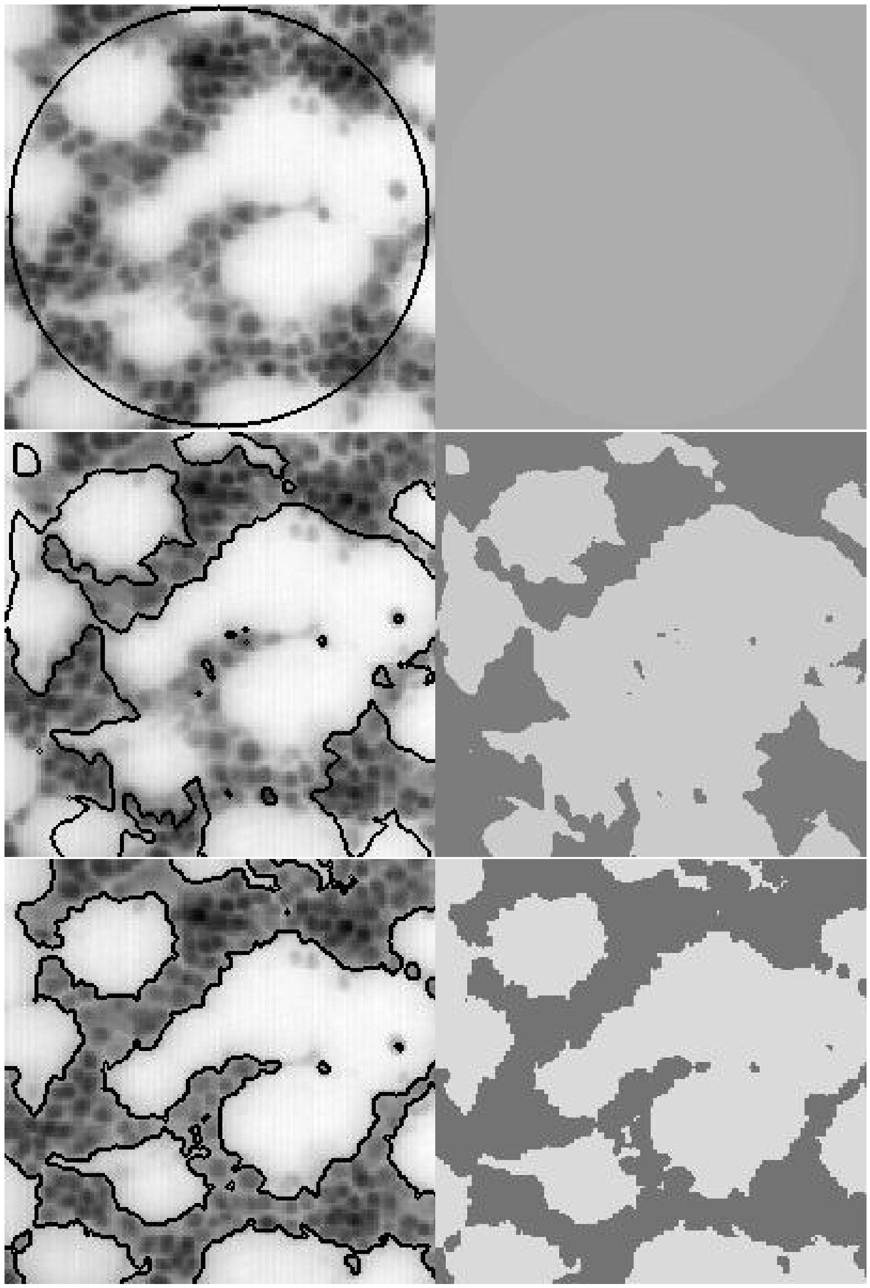

Fig. 1. The active contour model applied to a bone tissue image. Left: evolving contour. Right: corresponding two-phase piecewise-constant segmentation. The model can detect blurred edges and interior contours automatically, with automatic change of topology.

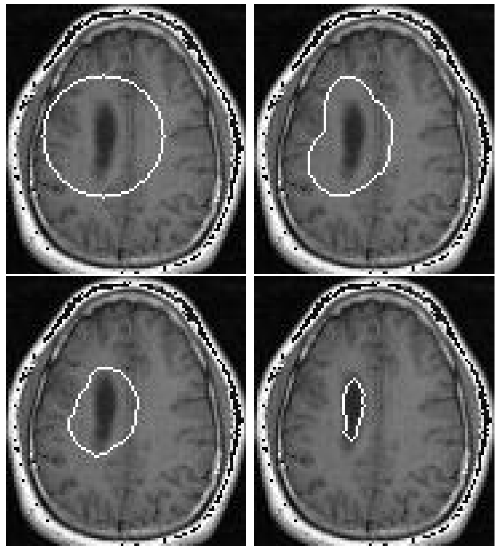

Fig. 2. Segmentation of a tumor in an MRI brain data, by the active contour model without edges. We show the evolution of the evolving contour, over the original image.

These methods allow for automatic detection of interior contours, and for segmentation of images with complex topologies into multiple segments, via a new multi-phase level set approach based segmentation. We have illustrated the efficiency of the proposed models by experimental results on 2D and 3D medical images.

Acknowledgments. The authors would like to thank the Editor, Dr. Ravi Malladi, for inviting us to contribute to this book. Also, we would like to thank Dr. Arthur W. Toga and Dr. Paul Thompson, from Laboratory of Neuro Imaging, Department of Neurology, and Dr. Sung-Cheng (Henry) Huang, from Molecular & Medical Pharmacology and Biomathematics, (UCLA School of Medicine), for providing us the MRI brain data, and for very useful discussions.

References

1. Ambrosio, L., Tortorelli, V.M.: Approximation of functionals depending on jumps by elliptic functionals via $\Gamma-$convergence. Comm. Pure Appl. Math. **43** (1990) 999–1036.
2. Ambrosio, L., Tortorelli, V.M.: On the Approximation of Free Discontinuity Problems. Bolletino U.M.I. **(7)6-B** (1992) 105–123.
3. Caselles, V., Catté, F., Coll, T., Dibos, F.: A geometric model for active contours in image processing. Numerische Mathematik **66** (1993) 1–31.

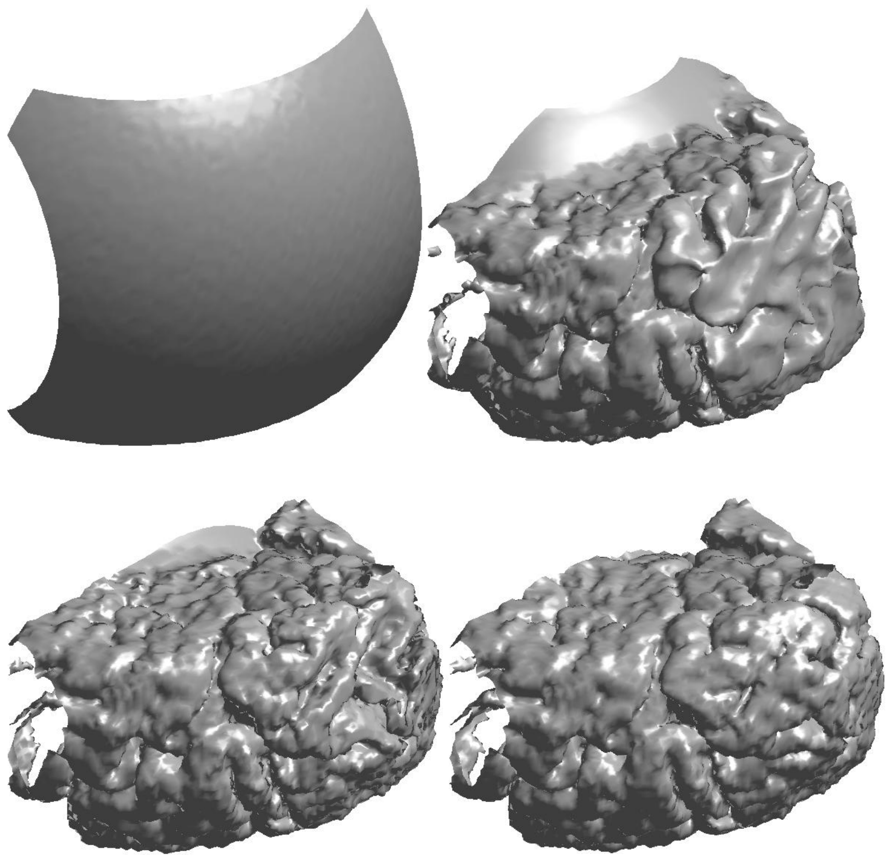

Fig. 3. Evolution of an active surface (using the 3D version of the active contour without edges), on a volumetric MRI brain data (we show here only a 61x61x61 cube from the 3D calculations performed on a larger domain, containing the brain.

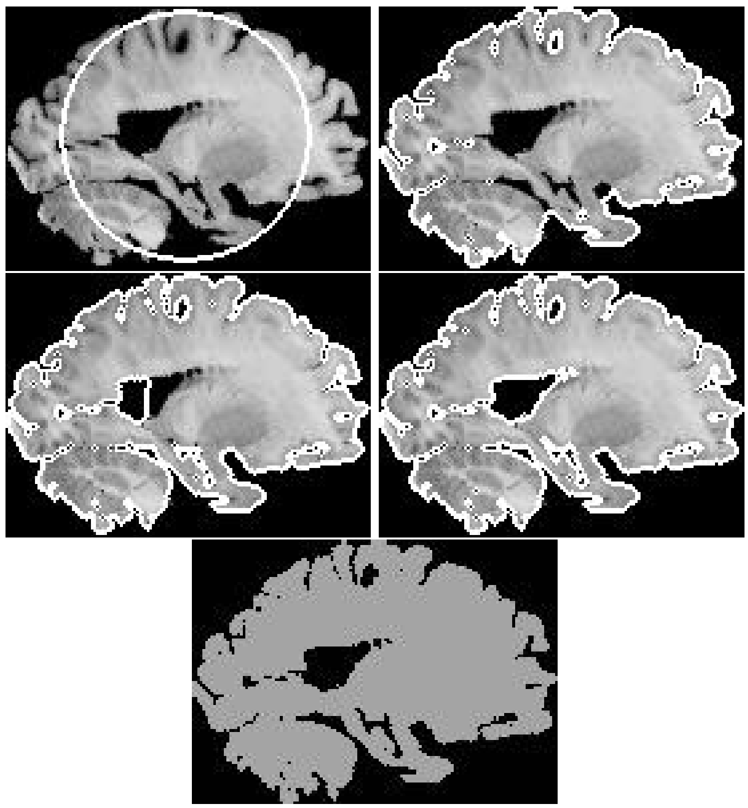

Fig. 4. Cross-sections of the previous 3D calculations, showing the evolving contour and the final segmentation on a slice of the volumetric image. We illustrate here how interior boundaries are automatically detected.

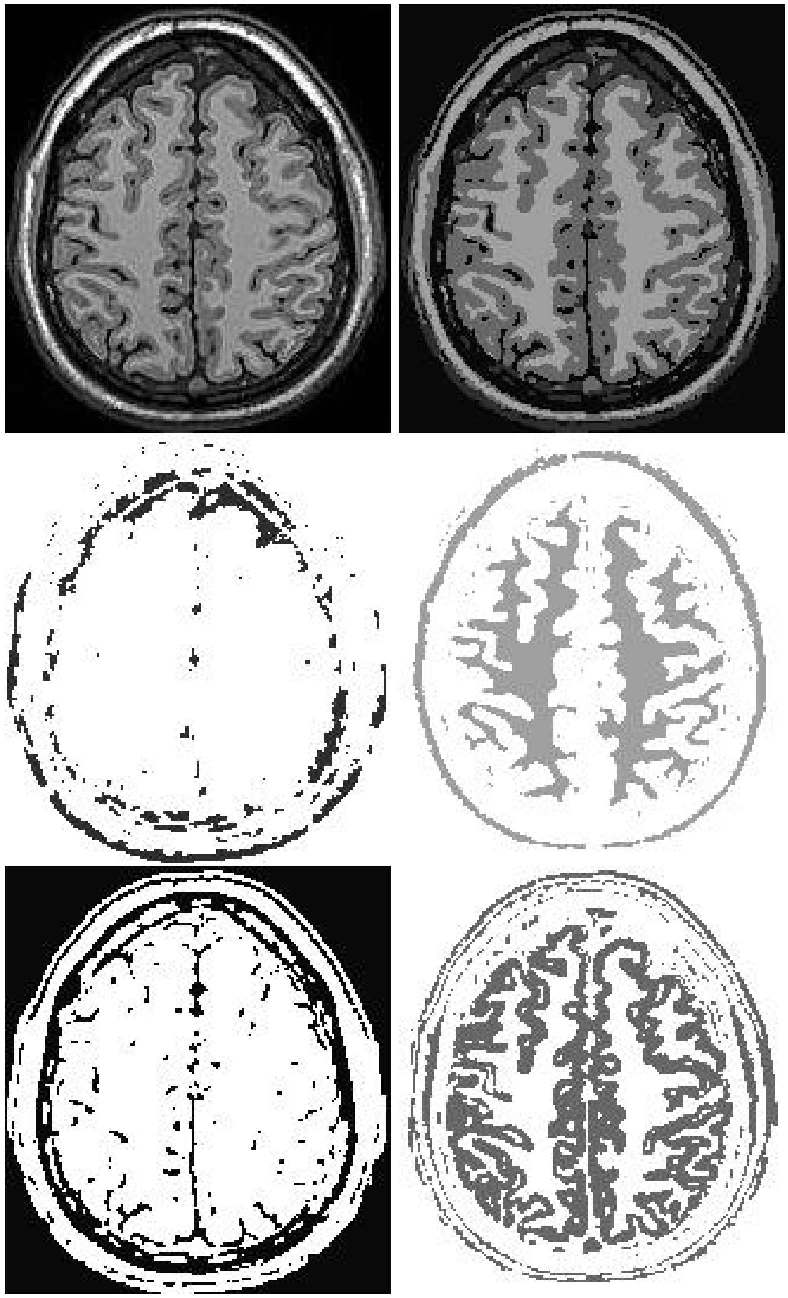

Fig. 5. Original & segmented images (top row); final segments (2nd, 3rd rows).

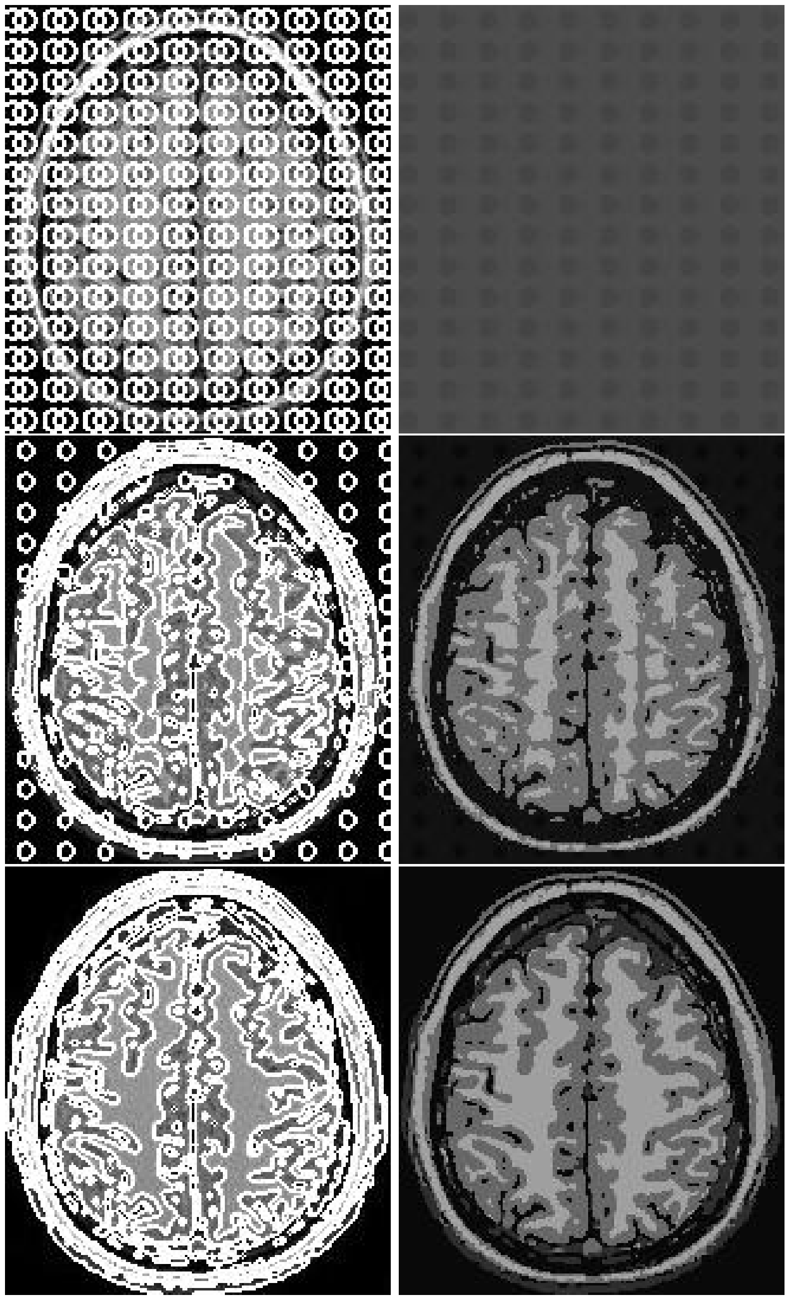

Fig. 6. Evolution of the four-phase segmentation model, using two level set functions. Left: the evolving curves. Right: corresponding piecewise-constant segmentations. Initialy, we seed the image with small circles, to obtain a very fast result.

4. Caselles, V., Kimmel, R., Sapiro, G.: On geodesic active contours. Int. J. of Computer Vision **22/1** (1997) 61–79.
5. Chambolle, A.: Image segmentation by variational methods: Mumford and Shah functional and the discrete approximations. SIAM J. Appl. Math. **55(3)** (1995) 827–863.
6. Chambolle, A.: Finite-differences discretizations of the Mumford-Shah functional. M2AN Math. Model. Numer. Anal. **33(2)** (1999) 261–288.
7. Chan, T., Vese, L.: Active contours without edges. IEEE Transactions on Image Processing. **10/2** (2001) 266–277.
8. Chan, T., Vese, L.: Image segmentation using level sets and the piecewise-constant Mumford-Shah model. UCLA CAM Report 00-14 (2000).
9. Kass, M., Witkin, A., Terzopoulos, D.: Snakes: Active contour models. Int. J. of Computer Vision **1** (1988) 321–331.
10. Kichenassamy, S., Kumar, A., Olver, P., Tannenbaum, A., Yezzi, A.: Gradient flows and geometric active contour models. Proceedings of ICCV, Cambridge, (1995) 810–815.
11. Kimmel, R., Malladi, R., Sochen, N.: Images as Embedded Maps and Minimal Surfaces: Movies, Color, Texture, and Volumetric Medical Images. International Journal of Computer Vision, **39/2** (2000) 111–129.
12. Koepfler, G., Lopez, C., Morel, J.M.: A multiscale algorithm for image segmentation by variational method. SIAM Journal of Numerical Analysis **31-1** (1994) 282–299.
13. Malladi, R., Kimmel, R., Adalsteinsson, D., Caselles, V., Sapiro, G., Sethian, J.A.: A Geometric Approach to Segmentation and Analysis of 3D Medical Images. Proc. of IEEE/SIAM Workshop on Biomedical Image Analysis, San-Francisco, California, (1996).
14. Malladi, R., Sethian, J.A.: A Real-Time Algorithm for Medical Shape Recovery. Proc. of International Conf. on Computer Vision. Mumbai, India (1998) 304–310.
15. Malladi, R., Sethian, J.A.: Level Set Methods for Curvature Flow, Image Enhancement, and Shape Recovery in Medical Images. Visualization and Mathematics, Eds. H. C. Hege, K. Polthier, Springer Verlag, Heidelberg (1997) 329–345.
16. Malladi, R., Sethian, J.A., Vemuri, B.C.: A Topology Independent Shape Modeling Scheme. Proc. SPIE Conf. on Geometric Methods in Computer Vision II **2031** (1993) 246–258, San Diego.
17. Malladi, R., Sethian, J.A., Vemuri, B.C.: Evolutionary Fronts for Topology-Independent Shape Modeling and Recovery. Proc. of the Third European Conference on Computer Vision, LNCS **800** (1994) 3–13, Stockholm, Sweden.
18. Malladi, R., Sethian, J.A., Vemuri, B.C.: Shape Modeling with Front Propagation: A Level Set Approach. IEEE Transactions on Pattern Analysis and Machine Intelligence. **17/2** (1995) 158–175.
19. March, R.: Visual Reconstruction with discontinuities using variational methods. Image and Vision Computing **10** (1992) 30–38.
20. Morel J.M., Solimini, S.: Variational Methods in Image Segmentation. Birkhäuser, PNLDE **14** (1994).
21. Mumford, D., Shah, J.: Optimal approximation by piecewise smooth functions and associated variational problems. Comm. Pure Appl. Math. **42** (1989) 577–685.

22. Osher, S., Sethian, J.A.: Fronts Propagating with Curvature-Dependent Speed: Algorithms Based on Hamilton-Jacobi Formulation. Journal of Computational Physics **79** (1988) 12–49.
23. Samson, C., Blanc-Féraud, L., Aubert, G., Zerubia, J.: A Level Set Model for Image Classification. M. Nilsen et al. (Eds.): Scale-Space'99, LNCS **1682** (1999) 306–317, Springer-Verlag Berlin Heidelberg.
24. Sapiro, G., Kimmel, R., Caselles, V.: Measurements in medical images via geodesic deformable contours. Proc. SPIE-Vision Geometry IV, Vol. **2573** (1995), San Diego, California.
25. Shah, J.: A Common Framework for Curve Evolution, Segmentation and Anisotropic Diffusion. IEEE Conference on Computer Vision and Pattern Recognition (1996).
26. Shah, J.: Riemannian Drums, Anisotropic Curve Evolution and Segmentation. M. Nilsen et al. (Eds.): Scale-Space'99, LNCS **1682** (1999) 129–140, Springer-Verlag Berlin Heidelberg.
27. Yezzi, A. Jr., Kichenassamy, S., Kumar, A., Olver, P., Tannenbaum, A.: A Geometric Snake Model for Segmentation of Medical Imagery. IEEE Transactions on Medical Imaging. **16/2** (1997) 199–209.
28. Yezzi, A., Tsai, A., Willsky, A.: A statistical approach to snakes for bimodal and trimodal imagery. Int. Conf. on Computer Vision (1999).
29. Zhao, H.-K., Chan, T., Merriman, B., Osher, S.: A Variational Level Set Approach to Multiphase Motion. J. Comput. Phys. **127** (1996) 179–195.
30. Zhu, S.C., Lee, T.S., Yuille, A.L.: Region competition: Unifying snakes, region growing, energy/Bayes/MDL for multi-band image segmentation. Proceedings of the IEEE 5th ICCV, Cambridge (1995) 416–423.
31. Zhu, S.C., Yuille, A.L.: Region competition: Unifying snakes, region growing, and Bayes/MDL for multi-band image segmentation. IEEE Transactions on Pattern Analysis and Machine Intelligence **18** (1996) 884–900.